Comput. Methods Appl. Mech. Engrg. 198 (2009) 1631–1637

Contents lists available at ScienceDirect

Comput. Methods Appl. Mech. Engrg.

journal homepage: www.elsevier.com/locate/cma

A macroscopic 1D model for shape memory alloys including asymmetric behaviors and transformation-dependent elastic properties

F. Auricchio [a,b,c], A. Reali [a,b,c,*], U. Stefanelli [c]

[a] Dipartimento di Meccanica Strutturale (DMS), Università degli Studi di Pavia, Via Ferrata 1, 27100 Pavia, Italy
[b] European Centre for Training and Research in Earthquake Engineering (EUCENTRE), Pavia, Italy
[c] Istituto di Matematica Applicata e Tecnologie Informatiche (IMATI), CNR, Pavia, Italy

ARTICLE INFO

Article history:
Received 31 October 2007
Received in revised form 25 September 2008
Accepted 20 January 2009
Available online 31 January 2009

Keywords:
Shape memory alloys
Tension–compression asymmetry
Variable elastic modulus
Phase transformation
Superelasticity
Shape-memory effect

ABSTRACT

The research toward an exhaustive modeling of the macroscopic behavior of shape memory alloys (SMAs) has been widely growing in last years because of the increasing employment of such smart materials in a large number of applications in many fields of engineering. Within this context, it has to be remarked that many models for SMAs available in the literature are able to properly reproduce main macroscopic SMA behaviors (i.e., superelasticity and shape-memory effect), without however modeling secondary effects that may turn out to be relevant in some practical cases. In this paper, we propose a new phenomenological one-dimensional model, which takes into account tension–compression asymmetries as well as elastic properties depending on the phase transformation level, combined with a good description of the superelastic and shape-memory behaviors. Moreover, we present some numerical tests showing model features and performance.

1. Introduction

The great and always increasing interest in shape memory alloys (SMAs) [5,6] and their industrial applications in the fields of aeronautical, biomedical, structural, and earthquake engineering are deeply stimulating the research on constitutive laws able to describe the behavior of these smart materials from a phenomenological point of view. In fact, there exist now many classes of devices (going from "micro" to "macro" scales) which are designed relying on one of the two characteristic SMA macroscopic behaviors: *superelasticity* (or *mechanical recovery*, i.e., the capability of recovering large stress-induced strains once the stress is removed) and *shape-memory effect* (or *thermal recovery*, i.e., the capability of recovering large stress-induced residual strains by heating the material); we refer the interested reader to [5,6] and references therein for a deeper description of such well-known effects.

Thus, many models able to reproduce one or both of the two SMA main macroscopic effects have been recently proposed in the literature in one or in three dimensions (see e.g. [7–15,18,20]). The purpose of such works is to give reliable models which could be used by engineers who need to construct simulation tools to design and study the response of SMA structures. To reach this goal, the proposed models have to be interfaced with analysis programs which are commonly used in engineering offices during the design process of a real device; accordingly, a good model should also be robust and flexible, possibly including both superelasticity and shape-memory effect, without becoming too complex.

Among the different models available in the recent literature, the one introduced in [16] and improved in [2] seems to be very attractive for its potential. Developed within the theory of irreversible thermodynamics, this model is in fact able to describe both superelasticity and shape-memory effect and the corresponding solution algorithm is simple and robust as it is based on a plasticity-like return map procedure. The robustness of such a model makes it particularly suitable for implementation within finite element codes, allowing in this way the simulation of the behavior of complex SMA devices.

However, in some applications also secondary effects not included in the model proposed in [2], such as the differences between the SMA response in tension and compression as well as the differences between the elastic properties at different phase transformation levels, can be relevant (see as an example Fig. 1, taken from [19]). It is then crucial to extend the model presented in [2] in order to take into account these secondary but important effects.

So, in the present work we propose a new phenomenological one-dimensional constitutive model able to describe classical

* Corresponding author. Address: Dipartimento di Meccanica Strutturale (DMS), Università degli Studi di Pavia, Via Ferrata 1, 27100 Pavia, Italy. Tel.: +39 0382 516937; fax: +39 0382 528422.
E-mail address: alessandro.reali@unipv.it (A. Reali).

0045-7825/$ - see front matter © 2009 Elsevier B.V. All rights reserved.
doi:10.1016/j.cma.2009.01.019

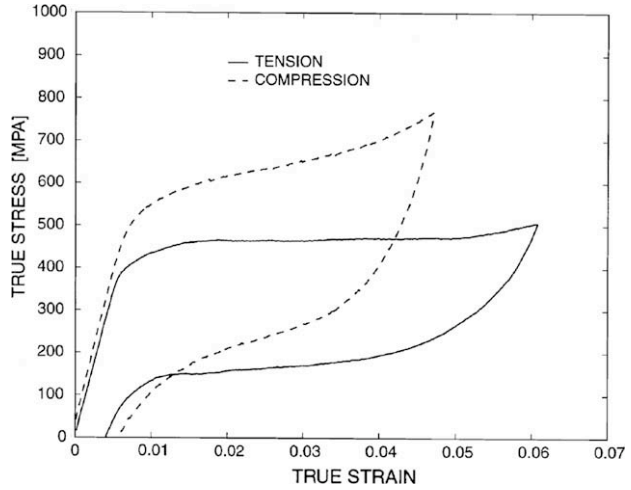

Fig. 1. Experimental stress–strain curves for a Ni–Ti SMA in simple tension and simple compression [19]. For compression the absolute values of stress and strain are plotted.

SMA macroscopic behaviors – including also tension–compression asymmetries in yield stress level as well as in loop width and length – and with an elastic modulus depending on the phase transformation level. In the following, we present an analytical description of the constitutive equations and we perform some numerical experiments to illustrate the model features. We finally highlight that the model can be easily generalized to the three-dimensional framework.

2. 1D model for stress-induced solid phase transformation

On the basis of the SMA constitutive model discussed in [2] and limiting the development to a 1D situation, we introduce an extended set of constitutive equations still capable of describing SMA macroscopic main behaviors, and also able to introduce and control some secondary but important effects such as tension–compression asymmetry (i.e., asymmetric yield stress level, loop width and length) and elastic properties depending on the reached phase transformation level.

We remark that all these extensions can be straightforwardly applied also to the constitutive model including permanent inelasticity presented in [3,4].

Moreover, we highlight that, in order to construct tension–compression asymmetric behaviors, in the model we make use of a modified norm, that can be easily extended to 3D settings with analogous results. In particular, instead of the standard norm (or, in 1D, the absolute value), we use the function denoted by $|\cdot|_i$, which is asymmetric and whose 3D extension can be, for example, the classical Prager-Lode J2/J3 norm (see, e.g., [2]). The definition of the new norm $|a|_i$ of a scalar a is

$$|a|_i = |a| + 2c_i(a)^- = (1+c_i)|a| - c_i a,$$

where $(a)^- = -(a-|a|)/2$ denotes the negative part function and c_i is a given constant. To ensure norm positivity, we have to select $c_i > -1/2$. In particular, for $c_i = 0$ the standard (symmetric) norm is recovered, while for $c_i > 0$ the slope for $a < 0$ is greater than that for $a > 0$.

The expression for the derivative of the asymmetric norm $|a|_i$ for $a \neq 0$ is

$$\frac{\mathrm{d}|a|_i}{\mathrm{d}a} = (1+c_i)\frac{\mathrm{d}|a|}{\mathrm{d}a} - c_i.$$

2.1. Time-continuous frame

The total strain ε is assumed as the control variable, while the transformation strain $\varepsilon^{\mathrm{tr}}$ is the only internal variable and plays the role of describing the strain associated to the phase transformation as in [2]. Moreover, we require

$$|\varepsilon^{\mathrm{tr}}|_1 \leqslant \varepsilon_L, \tag{2.1}$$

where ε_L is a material parameter corresponding to the maximum transformation strain reached at the end of the transformation and $c_1 \geqslant 0$ is a given constant.

Assuming a small strain regime, justified by the fact that the approximation of large displacements and small strains is valid for several applications, the free energy density function Ψ for a polycrystalline SMA material is expressed as the convex potential

$$\Psi(\varepsilon,\varepsilon^{\mathrm{tr}}) = \frac{1}{2}E(\varepsilon^{\mathrm{tr}})(\varepsilon-\varepsilon^{\mathrm{tr}})^2 + \beta(T-M_f)^+|\varepsilon^{\mathrm{tr}}|_2 + \frac{1}{2}h|\varepsilon^{\mathrm{tr}}|^2 + \mathscr{I}_{\varepsilon_L}(|\varepsilon^{\mathrm{tr}}|_1), \tag{2.2}$$

where $E(\varepsilon^{\mathrm{tr}})$ is the Young's modulus and is assumed to be depending on $\varepsilon^{\mathrm{tr}}$, and in particular on $|\varepsilon^{\mathrm{tr}}|_1$, as follows (see Remark 1 for more details on this choice)

$$E(\varepsilon^{\mathrm{tr}}) = \frac{\varepsilon_L}{\frac{\varepsilon_L - |\varepsilon^{\mathrm{tr}}|_1}{E_i} + \frac{|\varepsilon^{\mathrm{tr}}|_1}{E_f}} \tag{2.3}$$

being E_i and E_f (with $E_i \geqslant E_f$) the modulus values at the beginning and at the end of the phase transformation, respectively. We remark that, for the sake of notation simplicity, in the following we simply write E instead of $E(\varepsilon^{\mathrm{tr}})$. Moreover, $\beta \geqslant 0$ is a material parameter related to the dependence of the critical stress on the temperature, T is the absolute temperature, M_f is the temperature below which only martensite phase is stable, $c_2 \geqslant 0$, occurring in the definition of $|\cdot|_2$, is a given constant, and $h \geqslant 0$ is a material parameter controlling the slope of the linear stress–transformation strain relation. To satisfy the transformation strain constraint (2.1), in Eq. (2.2), we make use of the indicator function $\mathscr{I}_{\varepsilon_L}(|\varepsilon^{\mathrm{tr}}|_1)$, defined as

$$\mathscr{I}_{\varepsilon_L}(|\varepsilon^{\mathrm{tr}}|_1) = \begin{cases} 0 & \text{if } |\varepsilon^{\mathrm{tr}}|_1 \leqslant \varepsilon_L, \\ +\infty & \text{otherwise.} \end{cases}$$

We also define the positive part function as $(a)^+ = (a+|a|)/2$.

Following standard arguments, we can derive from the free energy density function Ψ the constitutive equations

$$\begin{cases} \sigma = \frac{\partial\Psi}{\partial\varepsilon} = E(\varepsilon-\varepsilon^{\mathrm{tr}}), \\ X = -\frac{\partial\Psi}{\partial\varepsilon^{\mathrm{tr}}} = \sigma - \frac{E'}{2}(\varepsilon-\varepsilon^{\mathrm{tr}})^2 - \beta(T-M_f)^+\frac{\mathrm{d}|\varepsilon^{\mathrm{tr}}|_2}{\mathrm{d}\varepsilon^{\mathrm{tr}}} - h\varepsilon^{\mathrm{tr}} - \gamma\frac{\mathrm{d}|\varepsilon^{\mathrm{tr}}|_1}{\mathrm{d}\varepsilon^{\mathrm{tr}}}, \end{cases} \tag{2.4}$$

where σ is the stress, while X is the thermodynamic stress-like quantity associated to the transformation strain $\varepsilon^{\mathrm{tr}}$. The variable γ results from the (sub)differentiation of the indicator function and fulfills

$$\begin{cases} \gamma = 0 & \text{if } |\varepsilon^{\mathrm{tr}}|_1 < \varepsilon_L, \\ \gamma \geqslant 0 & \text{if } |\varepsilon^{\mathrm{tr}}|_1 = \varepsilon_L. \end{cases}$$

The expression for the derivative E' of the elastic modulus follows from (2.3) and is

$$E' = \frac{\varepsilon_L\left(\frac{1}{E_i}-\frac{1}{E_f}\right)}{\left(\frac{\varepsilon_L-|\varepsilon^{\mathrm{tr}}|_1}{E_i}+\frac{|\varepsilon^{\mathrm{tr}}|_1}{E_f}\right)^2}\frac{\mathrm{d}|\varepsilon^{\mathrm{tr}}|_1}{\mathrm{d}\varepsilon^{\mathrm{tr}}}.$$

To control the evolution of the internal variable $\varepsilon^{\mathrm{tr}}$, we now introduce a limit function F defined as

$$F(X) = |X| - R[(1+c_3)\mathrm{sign}(\sigma) - c_3]^2, \tag{2.5}$$

where R is a material parameter defining the radius of the elastic domain and controlling the width of the hysteresis loops (cf. [2]) and $c_3 \geqslant 0$ is a given constant. We remark that we define the function sign as

$$\operatorname{sign}(\sigma) = \begin{cases} 1 & \text{if } \sigma \geqslant 0, \\ -1 & \text{otherwise,} \end{cases}$$

and hence the expression $(1+c_3)\operatorname{sign}(\sigma) - c_3$ in (2.5) is indeed $\frac{\mathrm{d}|\sigma|_3}{\mathrm{d}\sigma}$ except for the case $\sigma = 0$.

Considering then an associative framework, the flow rule for the internal variable takes the form

$$\dot{\varepsilon}^{\mathrm{tr}} = \dot{\zeta}\frac{\partial F}{\partial X} = \dot{\zeta}\frac{X}{|X|}. \tag{2.6}$$

We finally complete the model by the classical Kuhn–Tucker conditions

$$\begin{cases} \dot{\zeta} \geqslant 0, \\ F \leqslant 0, \\ \dot{\zeta}F = 0. \end{cases} \tag{2.7}$$

Remark 1. Fig. 1 shows that, for the specific alloy there considered, SMA behavior in tension and compression differs also in the secondary slopes (i.e., the slope of the transformation plateau). In the present work, such a difference is not taken into account, but, as done for other tension/compression behaviors, it could be included in the model by modifying the term $\frac{1}{2}h|\varepsilon^{\mathrm{tr}}|^2$ in Eq. (2.2) through the introduction of an asymmetric norm.

Remark 2. Different expressions for $E = E(\varepsilon^{\mathrm{tr}})$ have been proposed in the literature (see, e. g., [1]), the two most used being

$$E = \left(1 - \frac{|\varepsilon^{\mathrm{tr}}|}{\varepsilon_L}\right)E_i + \frac{|\varepsilon^{\mathrm{tr}}|}{\varepsilon_L}E_f,$$
$$E = \frac{\varepsilon_L}{\frac{\varepsilon_L - |\varepsilon^{\mathrm{tr}}|}{E_i} + \frac{|\varepsilon^{\mathrm{tr}}|}{E_f}}.$$

In this work, we use the latter expression (i.e., expression (2.3) with $|\cdot|$ replaced by $|\cdot|_1$) because we can prove the following claim.

Claim. For the proposed model, expression (2.3) is the right choice for $E = E(\varepsilon^{\mathrm{tr}})$, in the sense that it is the only function of $|\varepsilon^{\mathrm{tr}}|$ such that $\frac{\mathrm{d}\sigma}{\mathrm{d}\varepsilon} = 0$ when $h = 0$.

Starting with a generic function $E = E(\varepsilon^{\mathrm{tr}})$, let us compute the expression for the consistent tangent $\frac{\mathrm{d}\sigma}{\mathrm{d}\varepsilon}$ in the case

$$0 < |\varepsilon^{\mathrm{tr}}| < \varepsilon_L, \tag{2.8}$$
$$F = 0. \tag{2.9}$$

Moreover, for simplicity, we assume $c_1 = c_2 = c_3 = 0$ (this hypothesis is not however changing the implications of this argument). First of all, we differentiate Eq. $(2.4)_1$ with respect to time, obtaining

$$\dot{\sigma} = \frac{\mathrm{d}\sigma}{\mathrm{d}\varepsilon}\dot{\varepsilon} = E\dot{\varepsilon} - [E - E'(\varepsilon - \varepsilon^{\mathrm{tr}})]\dot{\varepsilon}^{\mathrm{tr}}. \tag{2.10}$$

To compute the consistent tangent, it is therefore clear that we need to evaluate $\dot{\varepsilon}^{\mathrm{tr}}$ as a function of $\dot{\varepsilon}$. Under condition (2.8), the residual equation related to the thermodynamic stress X reads as

$$\mathscr{R}^X = X - E(\varepsilon - \varepsilon^{\mathrm{tr}}) + \frac{E'}{2}(\varepsilon - \varepsilon^{\mathrm{tr}})^2 + \beta(T - M_f)^+\frac{\varepsilon^{\mathrm{tr}}}{|\varepsilon^{\mathrm{tr}}|} + h\varepsilon^{\mathrm{tr}} = 0. \tag{2.11}$$

Differentiating with respect to time, we obtain

$$\dot{\mathscr{R}}^X = \frac{\partial \mathscr{R}^X}{\partial \varepsilon^{\mathrm{tr}}}\dot{\varepsilon}^{\mathrm{tr}} + \frac{\partial \mathscr{R}^X}{\partial \varepsilon}\dot{\varepsilon} = 0,$$

which implies

$$\dot{\varepsilon}^{\mathrm{tr}} = -\frac{\partial \mathscr{R}^X}{\partial \varepsilon}\left(\frac{\partial \mathscr{R}^X}{\partial \varepsilon^{\mathrm{tr}}}\right)^{-1}\dot{\varepsilon}. \tag{2.12}$$

Note that, at this level, the above computation is just formal. However, a rigorous justification can be provided along the line of the forthcoming consistent tangent analysis.

The expressions for $\frac{\partial \mathscr{R}^X}{\partial \varepsilon^{\mathrm{tr}}}$ and $\frac{\partial \mathscr{R}^X}{\partial \varepsilon}$ are

$$\frac{\partial \mathscr{R}^X}{\partial \varepsilon^{\mathrm{tr}}} = E + h - 2E'(\varepsilon - \varepsilon^{\mathrm{tr}}) + \frac{E''}{2}(\varepsilon - \varepsilon^{\mathrm{tr}})^2,$$
$$\frac{\partial \mathscr{R}^X}{\partial \varepsilon} = -E + E'(\varepsilon - \varepsilon^{\mathrm{tr}}),$$

and, substituting them into (2.12), we finally obtain

$$\dot{\varepsilon}^{\mathrm{tr}} = \frac{E - E'(\varepsilon - \varepsilon^{\mathrm{tr}})}{E + h - 2E'(\varepsilon - \varepsilon^{\mathrm{tr}}) + \frac{E''}{2}(\varepsilon - \varepsilon^{\mathrm{tr}})^2}\dot{\varepsilon}. \tag{2.13}$$

We can now substitute Eq. (2.13) into Eq. (2.10) and collect $\dot{\varepsilon}$ as follows:

$$\dot{\sigma} = \frac{\mathrm{d}\sigma}{\mathrm{d}\varepsilon}\dot{\varepsilon} = \left\{E - \frac{[E - E'(\varepsilon - \varepsilon^{\mathrm{tr}})]^2}{E + h - 2E'(\varepsilon - \varepsilon^{\mathrm{tr}}) + \frac{E''}{2}(\varepsilon - \varepsilon^{\mathrm{tr}})^2}\right\}\dot{\varepsilon}.$$

We thus immediately obtain the expression for the consistent tangent, i.e.

$$\frac{\mathrm{d}\sigma}{\mathrm{d}\varepsilon} = E - \frac{[E - E'(\varepsilon - \varepsilon^{\mathrm{tr}})]^2}{E + h - 2E'(\varepsilon - \varepsilon^{\mathrm{tr}}) + \frac{E''}{2}(\varepsilon - \varepsilon^{\mathrm{tr}})^2}. \tag{2.14}$$

In the considered conditions, for the case $h = 0$, we expect a flat stress–strain response, i.e. $\frac{\mathrm{d}\sigma}{\mathrm{d}\varepsilon} = 0$. This assumption, in combination with Eq. (2.14), gives rise to the following equation:

$$E\left[E - 2E'(\varepsilon - \varepsilon^{\mathrm{tr}}) + \frac{E''}{2}(\varepsilon - \varepsilon^{\mathrm{tr}})^2\right] = [E - E'(\varepsilon - \varepsilon^{\mathrm{tr}})]^2,$$

which, assuming $\varepsilon \neq \varepsilon^{\mathrm{tr}}$, after simple computations reads as

$$EE'' = 2(E')^2. \tag{2.15}$$

Hence, we have checked that, by requiring the elastic modulus $\varepsilon^{\mathrm{tr}} \mapsto E(\varepsilon^{\mathrm{tr}})$ to be a function of $|\varepsilon^{\mathrm{tr}}|$ only, namely $E(\varepsilon^{\mathrm{tr}}) = e(|\varepsilon^{\mathrm{tr}}|)$, this last function e necessarily fulfills the nonlinear boundary value problem

$$ee'' - 2(e')^2 = 0 \quad \text{in } (0, \varepsilon_L), \tag{2.16}$$
$$e(0) = E_i, \quad e(\varepsilon_L) = E_f. \tag{2.17}$$

We then have the following result, proving that expression (2.3) is the optimal choice for $E = E(\varepsilon^{\mathrm{tr}})$.

Lemma. *The function $t \mapsto \varepsilon_L/[(\varepsilon_L - t)/E_i + t/E_f]$ is the only classical solution of the nonlinear boundary value problem (2.16) and (2.17).*

Proof. A direct check ensures that indeed $t \mapsto \varepsilon_L/[(\varepsilon_L - t)/E_i + t/E_f]$ solves (2.16) and (2.17). Hence, what we are left with is the uniqueness proof. To this aim, let a classical solution e of (2.16) and (2.17) be given and fix any $t_0 \in (0, \varepsilon_L)$ such that $e(t_0) > 0$ and $e'(t_0) < 0$. The latter t_0 of course exists as $E_i > E_f$. We observe that

$$f(t) = e(t_0)\left[1 - \frac{e'(t_0)}{e(t_0)}(t - t_0)\right]^{-1}$$

is the only solution in (a neighborhood of) $[t_0, \infty)$ of the Cauchy problem

$$ff'' - 2(f')^2 = 0, \quad f(t_0) = e(t_0), \quad f'(t_0) = e'(t_0). \tag{2.18}$$

Hence, $e(t) = f(t) = \alpha/(1+\beta t)$ for some $\alpha, \beta > 0$, at least on a right-semiline of the form $[s, \infty)$ where $s < t_0$.

Let now $r = \min\{t \geqslant 0 : e(t) = \alpha/(1+\beta t)\}$ and assume that $r > 0$. Then $e(r) = \alpha/(1+\beta r) > 0$ and $e'(r) = -\alpha\beta/(1+\beta r)^2 < 0$ by continuity. Hence, we can uniquely solve (2.18) with t_0 replaced by r, and prove that indeed $e(t) = \alpha/(1+\beta t)$ in a neighborhood of r as well, a contradiction.

Thus, we have proved that all solutions of (2.16) and (2.17) are of the form $e(t) = \alpha/(1+\beta t)$ for some $\alpha, \beta > 0$. Finally, the only choices ensuring $e(0) = E_i$ and $e(\varepsilon_L) = E_f$ are

$$\alpha = E_i, \quad \beta = (E_i - E_f)/(\varepsilon_L E_f),$$

whence the assertion follows. □

2.2. Time-discrete frame

We now introduce a subdivision of the time interval of interest $[0, t_f]$ and solve the evolution problem over the generic interval $[t_n, t_{n+1}]$ with $t_{n+1} > t_n$. Note that in the following, for the sake of notation simplicity, we drop the subindex $n+1$ for all the variables computed at time $t = t_{n+1}$.

We remark that the temperature is assumed to be assigned at each time step in order to treat only the mechanical part of the problem.

2.2.1. Time integration

Assumed to be given the solution at time t_n and the value of the total strain at time t, the implicit backward Euler scheme is employed to integrate the flow rules for the internal variables. In order to differentiate in zero the free energy Ψ, we substitute the norms $|\cdot|_i$ with $i = 1,2$ with their regularized version $\overline{|\cdot|}_i$ defined as

$$\overline{|a|}_i = \sqrt{|a|_i^2 + \delta_i} - \sqrt{\delta_i}, \tag{2.19}$$

where δ_i are user-defined positive small parameters controlling the regularization smoothness. We stress that, since we introduce a regularization only to obtain always differentiable functions and to guarantee the numerical robustness of the model, the parameter δ_i can be chosen very small (e.g., 10^{-8}).

Hence, the time-discrete constitutive model is finally written as

$$\begin{cases} \sigma = E(\varepsilon - \varepsilon^{\mathrm{tr}}), \\ X = \sigma - \frac{E'}{2}(\varepsilon - \varepsilon^{\mathrm{tr}})^2 - \beta(T - M_f)^+ \frac{\mathrm{d}\overline{|\varepsilon^{\mathrm{tr}}|}_2}{\mathrm{d}\varepsilon^{\mathrm{tr}}} - h\varepsilon^{\mathrm{tr}} - \gamma \frac{\mathrm{d}\overline{|\varepsilon^{\mathrm{tr}}|}_1}{\mathrm{d}\varepsilon^{\mathrm{tr}}}, \\ \varepsilon^{\mathrm{tr}} = \varepsilon^{\mathrm{tr}}_n + \Delta\zeta \frac{X}{|X|}, \\ F = |X| - R[(1+c_3)\mathrm{sign}(\sigma) - c_3]^2, \end{cases} \tag{2.20}$$

along with the requirements

$$\begin{cases} \gamma \geqslant 0, \\ \overline{|\varepsilon^{\mathrm{tr}}|}_1 \leqslant \varepsilon_L, \\ \Delta\zeta \geqslant 0, \quad F \leqslant 0, \quad \Delta\zeta F = 0, \end{cases} \tag{2.21}$$

where $\Delta\zeta = \zeta - \zeta_n = \int_{t_n}^{t_{n+1}} \dot{\zeta}\,\mathrm{d}t$ is the time-integrated consistency parameter.

2.2.2. Solution

The solution of the discrete model is performed by means of an elastic-predictor inelastic-corrector *return map* procedure as in classical plasticity problems [17]. An elastic trial state is evaluated for frozen internal variables and a trial value of the limit function is computed in order to check for the admissibility of the trial state. If the latter is not verified, the step is inelastic and the evolution equations are integrated.

As in [2], we distinguish two inelastic phases in our model: a non-saturated phase ($|\varepsilon^{\mathrm{tr}}|_1 < \varepsilon_L, \gamma = 0$) and a saturated one ($|\varepsilon^{\mathrm{tr}}|_1 = \varepsilon_L, \gamma \geqslant 0$). In our solution procedure we assume to be in a non-saturated phase, and at convergence we check if this assumption is violated. If the non-saturated solution is not admissible, then we search for a new solution under saturated conditions.

At each inelastic step, the nonlinear system constituted by Eq. (2.20) has to be solved. As the aim of this paper is to illustrate the model behavior (and not to focus on algorithmic problems), we find a solution to the system using the function *fsolve* implemented in the optimization toolbox of the program MATLAB®.

Finally, when dealing with superelastic problems at a fixed temperature $T = \overline{T}$, we would like to give a new set of input parameters, different from those used to describe the model, in order to simplify the parameter identification procedure. Hence, the goal is to rewrite the model without using the parameters $\varepsilon_L, \tau_m = \beta(\overline{T} - M_f)^+, R, c_1, c_2$, and c_3, but using instead the new parameters $\varepsilon_1, \varepsilon_2, \sigma_1, \sigma_2, \sigma_3$, and σ_4, that can be deduced in a simple way from a 1D superelastic tension–compression test (see Fig. 2, where the physical meaning of the different parameters is clearly indicated). So, we first write the new parameters using model Eqs. (2.1), (2.4) and (2.5) as follows:

$$\begin{cases} \varepsilon_1 = \varepsilon_L - \alpha\sigma_1, \\ \varepsilon_2 = \frac{\varepsilon_L}{1+2c_1} - \alpha\sigma_4, \\ \sigma_1 = \tau_m + R + \frac{E'(0^+)}{2}\varepsilon_{e1}^2, \\ \sigma_2 = \tau_m - R + \frac{E'(0^+)}{2}\varepsilon_{e2}^2, \\ \sigma_3 = \tau_m(1+2c_2) - R(1+2c_3)^2 + \frac{E'(0^-)}{2}\varepsilon_{e3}^2, \\ \sigma_4 = \tau_m(1+2c_2) + R(1+2c_3)^2 + \frac{E'(0^-)}{2}\varepsilon_{e4}^2 \end{cases} \tag{2.22}$$

with $\alpha = 1/E_i - 1/E_f, E'(0^+) = \alpha E_i^2/\varepsilon_L, E'(0^-) = (1+2c_1)\alpha E_i^2/\varepsilon_L$, and $\varepsilon_{ej} = \sigma_j/E_i (j = 1, \ldots, 4)$. Then, we compute the set of the old parameters as a function of the new ones, obtaining

$$\begin{cases} \varepsilon_L = \varepsilon_1 + \alpha\sigma_1, \\ \tau_m = \frac{\sigma_1+\sigma_2}{2} - \frac{\alpha}{4\varepsilon_L}(\sigma_1^2 + \sigma_2^2), \\ R = \frac{\sigma_1-\sigma_2}{2} - \frac{\alpha}{4\varepsilon_L}(\sigma_1^2 - \sigma_2^2), \\ c_1 = \frac{\varepsilon_L}{2(\varepsilon_2 + \alpha\sigma_4)} - \frac{1}{2}, \\ c_2 = \frac{\sigma_3+\sigma_4 - \frac{(1+2c_1)\alpha}{2\varepsilon_L}(\sigma_3^2+\sigma_4^2)}{4\tau_m} - \frac{1}{2}, \\ c_3 = \sqrt{\frac{\sigma_4 - \sigma_3 - \frac{(1+2c_1)\alpha}{2\varepsilon_L}(\sigma_4^2 - \sigma_3^2)}{8R}} - \frac{1}{2}. \end{cases} \tag{2.23}$$

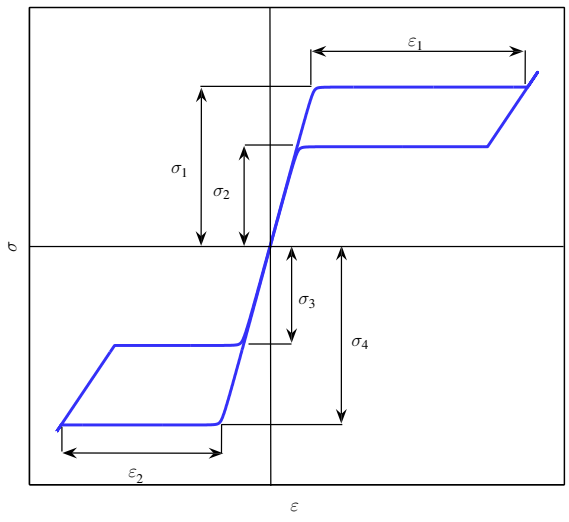

Fig. 2. Physical meaning of the new set of input parameters for superelasticity.

Table 1
Material parameters for the strain-driven superelastic test.

Parameter	E_f	ρ	E_i	h	σ_1	σ_2	σ_3	σ_4	ε_1	ε_2	$\delta_1 = \delta_2$
Value	2×10^4	150	5×10^4	0	400	250	250	450	4	3	10^{-8}
Unit	MPa	%	MPa	MPa	MPa	MPa	MPa	MPa	%	%	–

Remark 3. We highlight that the new parameters have been derived for the superelastic case at a constant temperature. For different situations (as it is the case of the shape-memory effect) the usual parameters have to be employed.

Remark 4. Another important observation is that when we deal with a temperature $T \leqslant M_f$ (i.e., when we are in the case of shape-memory effect), we expect to have a constant elastic modulus $E = E_f$, since only a martensite phase is present. This limit is reached gradually, so for low temperatures we expect values of E_i which are closer to E_f than what happens at higher temperatures. To include this in our model, we have to consider the dependence of the initial Young's modulus on the temperature. The relation we propose is the following

$$E_i(T) = E_f \left[1 + \rho \frac{(T - M_f)^+ - (T - M_s)^+}{M_s - M_f} \right]$$

with $\rho = \frac{E_i^*}{E_f} - 1$, where E_i^* is the initial modulus for $T \geqslant M_s$, and $M_s \geqslant M_f$ is the temperature at which austenite begins to transform into martensite at a constant stress level.

Finally, still referring to the case of shape-memory effect, we remark that the parameter c_2 is not affecting the model response, as it appears in a part of the energy which is zero in that case (cf. Eq. (2.2)).

3. Numerical results

In this section, we perform some numerical tests (both strain- and stress-driven) in order to illustrate model features. For every test, we represent the model response in terms of stress–strain curves.

We remark that, since every model parameter has a direct physical meaning which clearly shows its role within the model, we can avoid complex parametric studies. Accordingly, in the following we discuss only few fundamental numerical tests, with the sole aim of depicting the model capabilities in representing superelastic and shape-memory responses, enriched by the newly introduced secondary behaviors.

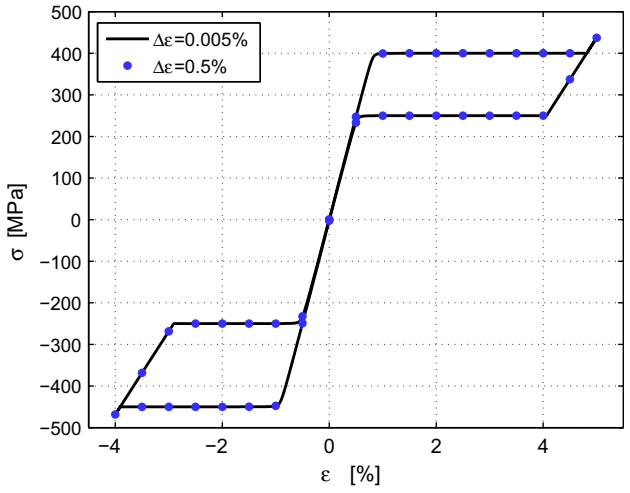

Fig. 3. Strain-driven superelastic test.

3.1. Strain-driven superelastic test

In this first test we describe a superelastic response using the material parameters represented in Fig. 2; the values used for the test are reported in Table 1. We impose a strain history which starts from zero, goes to 5%, then goes to −4% and finally returns back to a zero strain state. We perform the test using both fine (0.005%) and coarse (0.5%) strain step increments, in order to prove the robustness of the algorithm. The aim of the test is to show the performance and the robustness of the model in the superelastic case and to prove the simplicity of use of the proposed set of input parameters (very useful when one has to identify the material parameters from a superelastic experimental test). The obtained stress–strain response is plotted in Fig. 3.

3.2. Stress-driven tests at different temperatures

We now perform three stress-driven tests at different temperatures in order to show the capability of the model to describe both the superelastic and the shape-memory effect. Since we do not study only superelastic situations, we use the standard material parameters and we specify our choice in Table 2. The temperatures are different for the three cases and are selected as 293 K (superelastic case), 233 K (intermediate case), and 213 K (shape-memory case). We want again to prove the robustness of the algorithm, so we perform the tests using both fine (1 MPa) and coarse (40 MPa) stress step increments.

The input for the three cases are as follows:

- Superelastic case. Stress history: loading up to 320 MPa, then unloading up to −320 MPa, and reloading up to a zero stress state. Temperature: 293 K during the whole test.
- Intermediate case. Stress history: loading up to 200 MPa, then unloading up to −200 MPa, and reloading up to a zero stress state. Temperature: 233 K until the zero stress state is reached; then, keeping the stress constant, T is increased up to 293 K with 60 steps of 1 K each.
- Shape-memory case. Stress history: loading up to 200 MPa, then unloading up to −200 MPa, and reloading up to a zero stress state. Temperature: 213 K until the zero stress state is reached;

Table 2
Material parameters for the stress-driven tests at different temperatures.

Parameter	E_f	ρ	β	M_f	M_s	h	R	ε_L	c_1	c_2	c_3	$\delta_1 = \delta_2$
Value	2×10^4	150	2	223	239	1000	50	3	0.1	0.1	0.1	10^{-8}
Unit	MPa	%	MPa K^{-1}	K	K	MPa	MPa	%	–	–	–	–

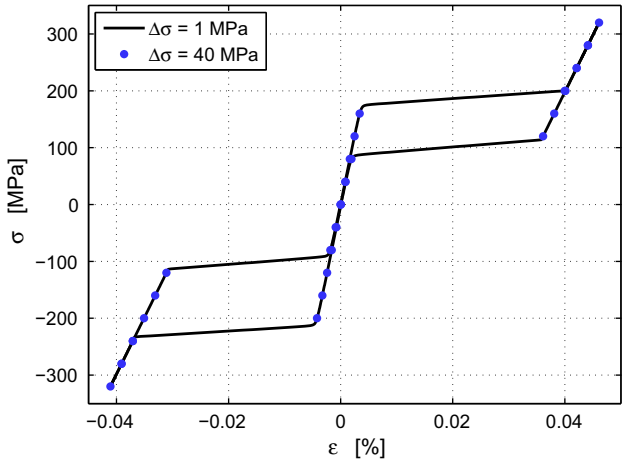

Fig. 4. Stress-driven test at $T = 293$ K.

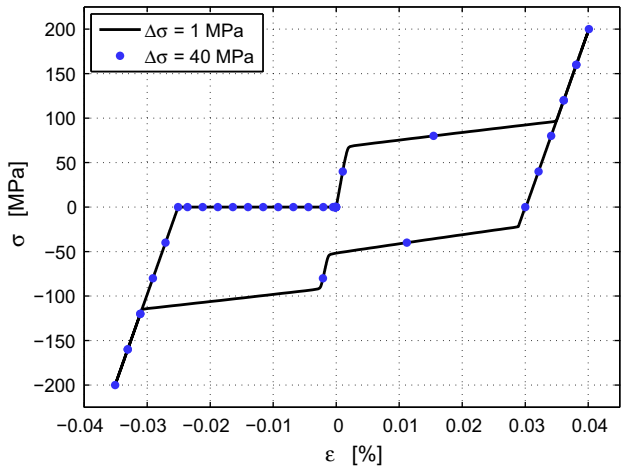

Fig. 5. Stress-driven test at $T = 233$ K with heating shape recovery.

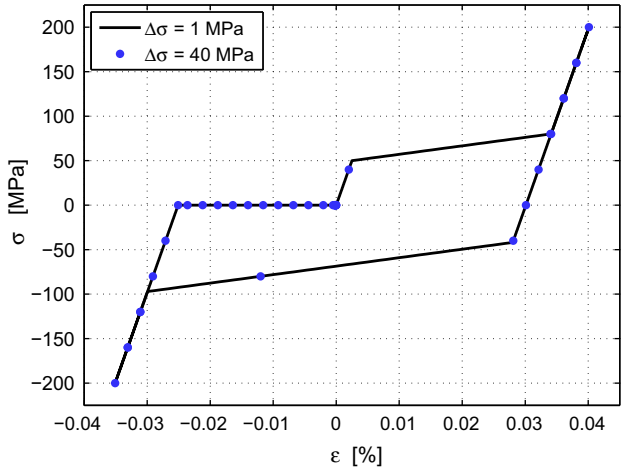

Fig. 6. Stress-driven test at $T = 213$ K with heating shape recovery.

then, keeping the stress constant, T is increased up to 293 K with 80 steps of 1 K each.

The obtained stress–strain curves are plotted in Figs. 4–6. It is possible to observe the good behavior of the model in all the three cases and its capability of representing tension–compression asymmetric behaviors as well as the dependence of the elastic modulus on the reached transformation strain level.

4. Conclusions

In this paper, we have introduced a new 1D constitutive model for describing the macroscopic behavior of SMAs. Compared with the model proposed in [2] (from which the present model takes its origin), it is capable of including a complete tension–compression asymmetric response (i.e., asymmetric yield stress level, loop width and length) as well as elastic properties depending on the reached phase transformation level. The good behavior of the model has been numerically tested and the performed numerical experiments have also shown the robustness of the proposed algorithm.

We finally remark that the present model could be naturally extended to 3D, while other possible future developments are the inclusion of permanent inelastic effects and of nonlinear hardening mechanisms. Also the discussion of a detailed algorithmic solution strategy, making possible to use the model to solve boundary value problems within a finite element code, will be the subject of future communications.

Acknowledgements

This work has been partially supported by Regione Lombardia through the INGENIO research program "Laser processing of SMA micro-devices"; by the Ministero dell'Università e della Ricerca (MiUR) through the PRIN research program "Shape memory alloy active microactuators and devices for biomedical applications: constitutive modeling, structural analysis, design, use of laser techniques for prototype implementation and experimental validation"; by the European Science Foundation through the EUROCORES S3T project "SMARTeR: Shape Memory Alloys to Regulate Transient Responses in civil engineering"; and by the European Research Council through the Starting Independent Research Grant "BioSMA: Mathematics for Shape Memory Technologies in Biomechanics".

References

[1] F. Auricchio, E. Sacco, A one-dimensional model for superelastic shape-memory alloys with different elastic properties between austenite and martensite, Int. J. Non-Linear Mech. 32 (1997) 1101–1114.
[2] F. Auricchio, L. Petrini, A three-dimensional model describing stress-temperature induced solid phase transformations. Part I: Solution algorithm and boundary value problems, Int. J. Numer. Methods Engrg. 61 (2004) 807–836.
[3] F. Auricchio, A. Reali, A phenomenological one-dimensional model describing stress-induced solid phase transformation with permanent inelasticity, Mech. Adv. Mater. Struct. 14 (2007) 43–55.
[4] F. Auricchio, A. Reali, U. Stefanelli, A three-dimensional model describing stress-induced solid phase transformation with permanent inelasticity, Int. J. Plast. 23 (2007) 207–226.
[5] T.W. Duerig, K.N. Melton, D. Stökel, C.M. Wayman (Eds.), Engineering Aspects of Shape Memory Alloys, Butterworth-Heinemann, 1990.
[6] T.W. Duerig, A.R. Pelton (Eds.), SMST-2003 Proceedings of the International Conference on Shape Memory and Superelastic Technology Conference, ASM International, 2003.
[7] S. Govindjee, C. Miehe, A multi-variant martensitic phase transformation model: formulation and numerical implementation, Comput. Methods Appl. Mech. Engrg. 191 (2001) 215–238.
[8] D. Helm, P. Haupt, Shape memory behaviour: modelling within continuum thermomechanics, Int. J. Solids Struct. 40 (2003) 827–849.
[9] D.C. Lagoudas, P.B. Entchev, P. Popov, E. Patoor, L.C. Brinson, X. Gao, Shape memory alloys, Part II: Modeling of polycrystals, Mech. Mater. 38 (2006) 391–429.
[10] P. Popov, D.C. Lagoudas, A 3-D constitutive model for shape memory alloys incorporating pseudoelasticity and detwinning of self-accommodated martensite, Int. J. Plast. 23 (2007) 1679–1720.
[11] V.I. Levitas, Thermomechanical theory of martensitic phase transformations in inelastic materials, Int. J. Solids Struct. 35 (1998) 889–940.

[12] B. Peultier, T. Ben Zineb, E. Patoor, Macroscopic constitutive law for SMA: application to structure analysis by FEM, Mater. Sci. Engrg.: A 438–440 (2006) 454–458.
[13] M. Peigney, A time-integration scheme for thermomechanical evolutions of shape-memory alloys, Comput. Rend. Mech. 334 (2006) 266–271.
[14] B. Raniecki, Ch. Lexcellent, R_L models of pseudoelasticity and their specification for some shape-memory solids, Eur. J. Mech., A: Solids 13 (1994) 21–50.
[15] S. Reese, D. Christ, Finite deformation pseudo-elasticity of shape memory alloys – constitutive modelling and finite element implementation, Int. J. Plast. (2007), doi:10.1016/j.ijplas.2007.05.005.
[16] A.C. Souza, E.N. Mamiya, N. Zouain, Three-dimensional model for solids undergoing stress-induced phase transformations, Eur. J. Mech., A: Solids 17 (1998) 789–806.
[17] J.C. Simo, T.J.R. Hughes, Computational Inelasticity, Springer-Verlag, 1998.
[18] E. Stein, O. Zwickert, Theory and finite element computations of a unified cyclic phase transformation model for monocrystalline materials at small strains, Comput. Mech. 40 (2007) 429–445.
[19] P. Thamburaja, L. Anand, Polycrystalline shape-memory materials: effect of crystallographic texture, J. Mech. Phys. Solids 49 (2001) 709–737.
[20] F. Thiebaud, Ch. Lexcellent, M. Collet, E. Foltete, Implementation of a model taking into account the asymmetry between tension and compression, the temperature effects in a finite element code for shape memory alloys structures calculations, Comput. Mater. Sci. (2007), doi:10.1016/j.commatsci.2007.04.006.